Inorganic Chemistry

Article

pubs.acs.org/IC

Synthesis and Magnetic Properties of a New Family of Macrocyclic $M^{II}_3Ln^{III}$ Complexes: Insights into the Effect of Subtle Chemical Modification on Single-Molecule Magnet Behavior

Humphrey L. C. Feltham,[†] Rodolphe Clérac,*[,‡,§] Liviu Ungur,[∥] Veacheslav Vieru,[∥] Liviu F. Chibotaru,*[,∥] Annie K. Powell,*[,⊥,#] and Sally Brooker*[,†]

[†]Department of Chemistry and the MacDiarmid Institute for Advanced Materials and Nanotechnology, University of Otago, P.O. Box 56, Dunedin, New Zealand

[‡]CNRS, CRPP, UPR 8641, F-33600 Pessac, France

[§]Univ. Bordeaux, CRPP, UPR 8641, F-33600 Pessac, France

[∥]Division of Quantum and Physical Chemistry, Katholieke Universiteit Leuven, Celestijenlaan 200F, 3001, Leuven, Belgium

[⊥]Institute of Inorganic Chemistry, Karlsruhe Institute of Technology, Engesserstraase 15 Geb. 30.45, 76131 Karlsruhe, Germany

[#]Institute for Nanotechnology, Karlsruhe Institute of Technology, Hermann-von-Helmholtz Platz 1, 76344 Eggenstein-Leopoldshafen, Germany

Supporting Information

ABSTRACT: Thirteen tetranuclear mixed-metal complexes of the hexaimine macrocycle $(\mathbf{L}^{Pr})^{6-}$ have been prepared in a one-pot 3:1:3:3 reaction of copper(II) acetate hydrate, the appropriate lanthanide(III) nitrate hydrate, 1,4-diformyl-2,3-dihydroxybenzene (**1**), and 1,3-diaminopropane. The resulting family of copper(II)−lanthanide(III) macrocyclic complexes has the general formula $Cu^{II}_3Ln^{III}(\mathbf{L}^{Pr})(NO_3)_3$·solvents (Ln = La, Ce, Pr, Nd, Sm, Eu, Gd, Dy, Tb, Ho, Er, Tm, or Yb). X-ray crystal structure determinations carried out on $[Cu_3Ce(\mathbf{L}^{Pr})(NO_3)_3(MeOH)_3]$ and $[Cu_3Dy(\mathbf{L}^{Pr})(NO_3)_3(MeOH)_3]$ confirmed that the large Ln^{III} ion is bound in the central O_6 site and the three square pyramidal Cu^{II} ions in the outer N_2O_2 sites (apical donor either nitrate anion or methanol molecule) of the Schiff base macrocycle. Only the structurally characterized Cu_3Tb complex, reported earlier, is a single-molecule magnet (SMM): the other 12 complexes do not exhibit an out-of-phase ac susceptibility signal or hysteresis of magnetization in a dc field. Ab initio calculations allowed us to rationalize the observed magnetic properties, including the significant impact of subtle chemical modification on SMM behavior. Broken-symmetry density functional theory (BS-DFT) calculations show there is a subtle structural balance as to whether the Cu···Cu exchange coupling is ferro- or antiferromagnetic. Of the family of 13 magnetically characterized tetranuclear $Cu^{II}_3Ln^{III}$ macrocyclic complexes prepared, only the Tb^{III} complex is an SMM: the theoretical reasons for this are discussed.

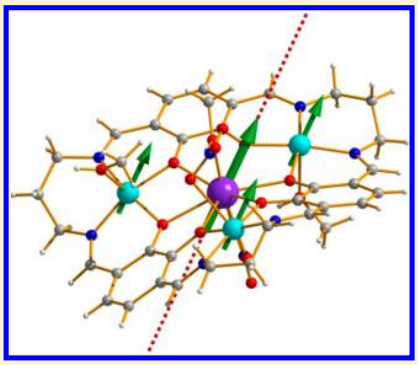

INTRODUCTION

The term single-molecule magnet (SMM) is used to describe systems which show slow relaxation of magnetization of purely molecular origin, behaving effectively like tiny magnets. Thus, at sufficiently low temperatures, SMMs can become trapped in an energetically favored 'total spin up' or 'total spin down' ($M_S = \pm S_T$) state for a significant period of time.[1] This may ultimately permit them to be used as components for molecular-scale data storage. The fact that they are of a molecular dimension also means that quantum effects, such as tunneling of the magnetization, can become important with possible applications in data processing.[2] An important current challenge in SMM research aimed toward applications in data storage is to increase the blocking temperature (defined for a 1 s experimental time scale) above the current record of 14 K.[3]

Many SMMs are prepared by complexing acyclic ligands with 3d metal ions,[4] 4f metal ions,[5] or both.[5,6] While this approach can and does yield magnetically interesting complexes,[7] characterization relies on growing single crystals of the product for X-ray crystallography in order to determine the nuclearity and structural details of the resulting coordination complex, both of which are difficult if not impossible to predict with any confidence.

An attractive alternative is to use organic macrocyclic ligands with enough binding pockets to accommodate several metal ions. Such macrocycles can also be designed so that they provide specific binding pockets favoring different types of metal ions, greatly facilitating controlled formation of mixed-

Received: April 20, 2012
Published: September 24, 2012

metal complexes. Thus, employing large macrocyclic ligands opens up the possibility of accessing a new generation of 3d−4f SMMs with prescribed nuclearity and structure. The binding pockets can not only be tailored to suit the coordination preferences of the targeted metal ions but also, as we have already discovered, influence the orientation of the anisotropy axes.[8] In the case of lanthanide ions, the uniaxial anisotropy depends of the shape of the 4f electron density and the arrangement of the donor atoms around the ion; some ligand fields result in pronounced magnetic anisotropy by stabilizing certain M_J states relative to others.[9] Hence, another strength of the large macrocycle approach is that it facilitates preparation of a large series of analogous complexes in which only the Ln^{III} ion (and hence the shape of the 4f electron density) is varied,[8a,10] allowing determination of which 4f ion is best suited to a particular binding pocket. Furthermore, the macrocyclic complexes should be soluble and, importantly, stay intact in solution. This would enable future processing, deposition, and solution state studies, all of which offer a practical means of realizing future application of SMMs. Finally, the organic bulk of the macrocycle can help to minimize or even prevent undesirable intermolecular magnetic interactions. The fact that the macrocycle controls and hence limits the nuclearity of the complex is advantageous for two reasons. First, this allows an exploration of the utility of employing certain blends of 3d/4f metal ions within a constrained and structure-directing environment, and second, following on from this, it makes it possible to test the premise that higher blocking temperatures will result from a fine control of anisotropy rather than by simply trying to achieve large ground spin states.[11]

Smaller, single-binding-site organic macrocycles have been successfully used, mostly by Ishikawa and co-workers, to prepare mononuclear SMMs containing a single, eight-coordinate lanthanide ion sandwiched between two N_4 phthalocyanine macrocycles.[12] We decided to use our experience[13] working with larger, multiple-binding-site, organic macrocycles to create 3d−4f coordination complexes in a controlled manner. Accordingly, a family of tetranuclear $Zn^{II}_3Ln^{III}$ complexes of a hexaimine [3 + 3] macrocycle $(\mathbf{L}^{Pr})^{6-}$ was prepared[8a,10] using one-pot metal-templated reactions of the dialdehyde 1,4-diformyl-2,3-dihydroxybenzene (**1**) with 1,3-diaminopropane. This design was inspired by the macrocycles reported by the MacLachlan[14] and Nabeshima[15] groups,[16] in particular, the oxime macrocycle $H_6\mathbf{L}^{Ox}$ reported by Nabeshima and co-workers in 2007 (Figure 1).[17]

Within the $Zn^{II}_3Ln^{III}(\mathbf{L}^{Pr})$ family, the complex $[Zn_3Dy(\mathbf{L}^{Pr})(NO_3)_3(MeOH)_3]\cdot 4H_2O$ was established to be the first example of this new class of SMM, in which a single lanthanide ion is coordinated within the designed cavity of a single organic macrocyclic ligand, surrounded by three 3d metal ions, also within the cavity, in an approximately trigonal array.[8a] Such a structural motif was already known for acyclic ligands,[18] but our design and use of the $(\mathbf{L}^{Pr})^{6-}$ macrocycle provides many advantages, as outlined above. Kajiwara, Nabeshima, and co-workers recently reported the second example of such a SMM, specifically a $Zn^{II}_3Er^{III}$ complex of a related macrocycle, $(\mathbf{L}^{Ph})^{6-}$ (Figure 1),[19] confirming the promise of this new macrocyclic approach to generating SMMs.

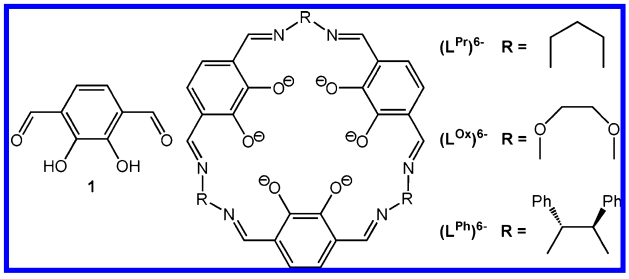

Figure 1. Dialdehyde **1** and macrocyles $(\mathbf{L}^{Pr})^{6-}$, $(\mathbf{L}^{Ox})^{6-}$, and $(\mathbf{L}^{Ph})^{6-}$. Of these macrocycles, $(\mathbf{L}^{Ox})^{6-}$ has also been isolated as the free ligand $H_6\mathbf{L}^{Ox}$.

Pleasingly, we found that the macrocycle can also be formed via a template reaction using a combination of three Cu^{II} ions and one Ln^{III} ion,[20] allowing exploration of the effect of incorporating paramagnetic 3d centers without the need to prepare the metal-free macrocycle $H_6\mathbf{L}^{Pr}$ or to transmetallate a Zn^{II} complex of the macrocycle. Here, having recently reported the synthesis, structure, and SMM properties of the $Cu^{II}_3Tb^{III}$ complex of this macrocycle, which is the third example of such an SMM,[20] we report the synthesis and characterization of a family of 13 analogues, $Cu^{II}_3Ln^{III}(\mathbf{L}^{Pr})(NO_3)_3\cdot x$solvents, in which the lanthanide ion can and is varied at will. Such a systematic variation, in which all features of the system are preserved apart from the electronic nature of the 4f ion, provides invaluable insights into the features required for creating molecular magnets. These families of isostructural complexes demonstrate that SMM behavior can be lost on minor chemical modification, and ab initio calculations allow these observations to be rationalized.

EXPERIMENTAL SECTION

General. All chemicals were of A. R. Grade and used as received. Compound **1** was prepared in two steps from veratrole, as reported earlier.[10,21] IR spectra were recorded as solids on a Bruker Alpha FT-ATR IR spectrometer with a diamond anvil Alpha-P module between 400 and 4000 cm^{-1}. ESI-MS data were collected with a Bruker MicrOTOF$_Q$ spectrometer using MeOH. Microanalysis was carried out by the Campbell Microanalytical Laboratory at the University of Otago.

Single-crystal X-ray measurements were carried out on a Bruker SMART Apex diffractometer using graphite-monochromated Mo Kα radiation (λ = 0.71073 Å). Structure solution and full-matrix least-squares refinement were carried out using the SHELXTL software package.[22] All non-H atoms were assigned anisotropic thermal parameters, except for the disordered atoms in the structure of $[Cu_3Dy(\mathbf{L}^{Pr})(NO_3)_3(MeOH)_3]$. H atoms bonded to C atoms were placed in calculated positions, while those on O atoms were placed in calculated positions that gave the best hydrogen bonds. For further details see the cif files.

Crystal data for $[Cu_3Ce(\mathbf{L}^{Pr})(NO_3)_3(MeOH)_3]$: Triclinic, *P*-1, dark green rod, a = 10.581(3) Å, b = 13.203(3) Å, c = 15.696(5) Å, α = 80.395(7)°, β = 78.989(7)°, γ = 76.962(8)°, V = 2079.1(8) Å^3, Z = 2, T = 92 K. Structure was solved by direct methods (SHELXS-97)[22] and refined against all 8902 unique F^2 data (SHELXL)[22] to wR^2 = 0.1181, GooF = 1.048; for the 7869 data with $F > 4\sigma(F)$, R^1 = 0.0427. CCDC 829375.

Crystal data for $[Cu_3Dy(\mathbf{L}^{Pr})(NO_3)_3(MeOH)_3]$: Triclinic, *P*-1, brown irregular block, a = 12.1722(14) Å, b = 13.4004(14) Å, c = 14.7438(14) Å, α = 109.487(5)°, β = 95.676(5)°, γ = 110.021(5)°, V = 2067.5(4) Å^3, Z = 2, T = 92 K. Structure was solved by direct methods (SHELXS-97)[22] and refined against all 9970 unique F^2 data (SHELXL)[22] to wR^2 = 0.1181, GooF = 1.057; for the 8511 data with $F > 4\sigma(F)$, R^1 = 0.0464. CCDC 829374.

Magnetic susceptibility measurements were obtained using an MPMS-XL Quantum Design SQUID magnetometer operating between 1.8 and 400 K for dc applied fields ranging from −70 to 70 kOe. Measurements were performed on polycrystalline samples

dx.doi.org/10.1021/ic300819u | *Inorg. Chem.* 2012, 51, 10603−10612

which were loaded into a polyethylene bag (3 × 0.5 × 0.02 cm) and sealed under argon. The ac susceptibility measurements were measured with an oscillating ac field of 3 Oe with frequencies between 1 and 1500 Hz. Magnetic data were corrected for the sample holder and diamagnetic contributions.

Synthesis. *General Synthetic Method for $Cu_3Ln(L^{Pr})(NO_3)_3{\cdot}x$solvents.* To a solution of **1** (0.030 g, 0.18 mmol) in methanol (5 mL) was added $Cu(OAc)_2{\cdot}H_2O$ (0.036 g, 0.18 mmol) suspended in a solution of $Ln(NO_3)_3{\cdot}xH_2O$ (0.06 mmol, Ln = La, Ce, Pr, Nd, Sm, Eu, Gd, Tb, Dy, Ho, Er, Tm, or Yb) in MeOH (10 mL), resulting in a dark brown solution. After stirring this solution for 2 h, 1,3-diaminopropane (0.014 g, 0.18 mmol) in methanol (5 mL) was added, resulting in a green-brown solution. This solution was stirred for a further 10 min and left to stand overnight. Diethyl ether was then vapor diffused into the solution, resulting in precipitation of a solid. The solid was filtered, washed with diethyl ether, and dried in air, giving $Cu_3Ln(\mathbf{L}^{Pr})(NO_3)_3{\cdot}x$solvents.

$Cu_3La(L^{Pr})(NO_3)_3{\cdot}3MeOH{\cdot}H_2O$. Reported in ref 20.

$[Cu_3Ce(L^{Pr})(NO_3)_3(MeOH)(H_2O)_2]{\cdot}H_2O$. Brown powder (0.037 g, 51%). Anal. Calcd for $Cu_3CeC_{34}H_{38}N_9O_{18}{\cdot}H_2O$: C, 34.78; H, 3.57; N, 10.14. Found: C, 33.50; H, 3.05; N, 10.11. ESI-MS (m/z) = 1061.9 $[Cu_3Ce(\mathbf{L}^{Pr})(NO_3)]^+$, 499.5 $[Cu_3Ce(\mathbf{L}^{Pr})(NO_3)]^{2+}$, 312.3 $[Cu_3Ce(\mathbf{L}^{Pr})]^{3+}$. IR (FT-ATR diamond anvil) $\bar{\nu}/cm^{-1}$ = 1618 (m); 1523 (w); 1458 (m); 1411 (w); 1321 (s); 1264 (m); 1231 (s); 1187 (m); 1082 (m); 1041 (m); 973 (w); 888 (w); 860 (w); 817 (w); 782 (m); 737 (s); 642 (m); 602 (s); 545 (m); 504 (m).

$Cu_3Pr(L^{Pr})(NO_3)_3{\cdot}MeOH{\cdot}4H_2O$. Brown powder (0.034 g, 59%). Anal. Calcd for $Cu_3PrC_{34}H_{38}N_9O_{20}$: C, 33.25; H, 3.45; N, 10.26. Found: C, 33.48; H, 2.91; N, 9.80. ESI-MS (m/z) = 1061.9 $[Cu_3Pr(\mathbf{L}^{Pr})(NO_3)_2]^+$, 499.9 $[Cu_3Pr(\mathbf{L}^{Pr})(NO_3)]^{2+}$, 312.7 $[Cu_3Pr(\mathbf{L}^{Pr})]^{3+}$. IR (FT-ATR diamond anvil) $\bar{\nu}/cm^{-1}$ = 1615 (m); 1523 (w); 1458 (m); 1412 (w); 1324 (s); 1259 (m); 1232 (s); 1185 (m); 1081 (m); 1044 (m); 974 (w); 887 (w); 870 (w); 819 (w); 787 (m); 738 (s); 643 (m); 602 (s); 545 (m); 504 (m).

$Cu_3Nd(L^{Pr})(NO_3)_2{\cdot}5H_2O$. Brown powder (0.043 g, 59%). Anal. Calcd for $Cu_3NdC_{33}H_{40}N_9O_{20}$: C, 32.55; H, 3.31; N, 10.35. Found: C, 32.58; H, 3.21; N, 10.05. ESI-MS (m/z) = 501.4 $[Cu_3Nd(\mathbf{L}^{2})(NO_3)]^{2+}$, 313.6 $[Cu_3Nd(\mathbf{L}^{Pr})]^{3+}$. IR (FT-ATR diamond anvil) $\bar{\nu}/cm^{-1}$ = 1614 (m); 1523 (w); 1459 (m); 1412 (w); 1323 (s); 1258 (m); 1232 (m); 1184 (m); 1081 (m); 1046 (m); 975 (w); 885 (w); 870 (w); 818 (w); 787 (m); 738 (s); 643 (m); 602 (s); 545 (m); 505 (m).

$Cu_3Sm(L^{Pr})(NO_3)_3{\cdot}MeOH{\cdot}2H_2O$. Prepared on a 0.05 g of **1** (instead of 0.03 g) scale. Brown powder (0.05 g, 42%). Anal. Calcd for $Cu_3SmC_{34}H_{38}N_9O_{18}$: C, 33.98; H, 3.19; N, 10.49. Found: C, 34.21; H, 3.02; N, 10.57. ESI-MS (m/z) = 1072.9 $[Cu_3Sm(\mathbf{L}^{Pr})(NO_3)_2]^+$, 505.5 $[Cu_3Sm(\mathbf{L}^{Pr})(NO_3)]^{2+}$. IR (FT-ATR diamond anvil) $\bar{\nu}/cm^{-1}$ = 1614 (m); 1523 (w); 1458 (m); 1410 (w); 1322 (s); 1263 (m); 1232 (m); 1187 (m); 1080 (m); 1036 (m); 976 (w); 888 (w); 859 (w); 817 (w); 781 (m); 739 (s); 641 (m); 602 (s); 546 (m); 503 (m).

$Cu_3Eu(L^{Pr})(NO_3)_3{\cdot}MeOH{\cdot}3H_2O$. Brown powder (0.037 g, 50%). Anal. Calcd for $Cu_3EuC_{34}H_{40}N_9O_{19}$: C, 32.44; H, 3.30; N, 10.32. Found: C, 33.60; H, 2.90; N, 10.21. ESI-MS (m/z) = 505.0 $[Cu_3Eu(\mathbf{L}^{Pr})(NO_3)]^{2+}$, 316.0 $[Cu_3Eu(\mathbf{L}^{Pr})]^{3+}$. IR (FT-ATR diamond anvil) $\bar{\nu}/cm^{-1}$ = 1618 (m); 1523 (w); 1458 (m); 1406 (w); 1321 (s); 1263 (m); 1232 (m); 1187 (m); 1080 (m); 1036 (m); 974 (w); 888 (w); 861 (w); 818 (w); 778 (m); 739 (s); 642 (m); 600 (s); 546 (m); 503 (m).

$Cu_3Gd(L^{Pr})(NO_3)_3{\cdot}MeOH{\cdot}3H_2O$. Brown powder (0.043 g, 58%). Anal. Calcd for $Cu_3GdC_{34}H_{40}N_9O_{19}$: C, 33.29; H, 3.29; N, 10.28. Found: C, 33.25; H, 2.78; N, 9.76. ESI-MS (m/z) = 508.5 $[Cu_3Gd(\mathbf{L}^{Pr})(NO_3)]^{2+}$, 318.3 $[Cu_3Er(\mathbf{L}^{Pr})]^{3+}$. IR (FT-ATR diamond anvil) $\bar{\nu}/cm^{-1}$ = 1615 (m); 1524 (w); 1460 (m); 1407 (w); 1323 (s); 1258 (m); 1233 (m); 1185 (m); 1082 (m); 1040 (m); 975 (w); 885 (w); 869 (w); 818 (w); 786 (m); 739 (s); 643 (m); 601 (s); 545 (m); 503 (m).

$[Cu_3Tb(L^{Pr})(NO_3)_2(H_2O)_2(MeOH)](NO_3){\cdot}3H_2O$. Reported in ref 20.

$[Cu_3Dy(L^{Pr})(NO_3)_3(MeOH)_2(H_2O)]{\cdot}3H_2O$. Brown powder (0.037 g, 48%). Anal. Calcd for $Cu_3DyC_{35}H_{46}N_9O_{21}$: C, 32.79; H, 3.62; N, 9.83. Found: C, 32.52; H, 3.39; N, 9.84. ESI-MS (m/z) = 510.5 $[Cu_3Dy(\mathbf{L}^{Pr})(NO_3)]^{2+}$, 319.6 $[Cu_3Dy(\mathbf{L}^{Pr})]^{3+}$. IR (FT-ATR diamond anvil) $\bar{\nu}/cm^{-1}$ = 1617 (m); 1526 (w); 1460 (m); 1409 (w); 1327 (s); 1262 (m); 1233 (m); 1188 (m); 1081 (m); 1035 (m); 975 (w); 887 (w); 860 (w); 818 (w); 780 (m); 740 (s); 642 (m); 600 (s); 545 (m); 501 (m).

$Cu_3Ho(L^{Pr})(NO_3)_3{\cdot}MeOH{\cdot}3H_2O$. Brown powder (0.036 g, 49%). Anal. Calcd for $Cu_3HoC_{34}H_{40}N_9O_{19}$: C, 33.09; H, 3.27; N, 10.21. Found: C, 33.19; H, 2.90; N, 9.86. ESI-MS (m/z) = 512.1 $[Cu_3Ho(\mathbf{L}^{Pr})(NO_3)]^{2+}$, 320.6 $[Cu_3Ho(\mathbf{L}^{Pr})]^{3+}$. IR (FT-ATR diamond anvil) $\bar{\nu}/ cm^{-1}$ = 1615 (m); 1524 (w); 1461 (m); 1409 (w); 1323 (s); 1258 (m); 1233 (m); 1186 (m); 1095 (m); 1081 (m); 1039 (m); 975 (w); 886 (w); 870 (w); 818 (w); 782 (m); 739 (s); 642 (m); 599 (s); 545 (m); 504 (m).

$Cu_3Er(L^{Pr})(NO_3)_3{\cdot}MeOH{\cdot}3H_2O$. Brown powder (0.035 g, 47%). Anal. Calcd for $Cu_3ErC_{34}H_{40}N_9O_{19}$: C, 33.02; H, 3.26; N, 10.19. Found: C, 32.92; H, 2.97; N, 10.08. ESI-MS (m/z) = 1088.9 $[Cu_3Er(\mathbf{L}^{Pr})(NO_3)_2]^+$, 513.5 $[Cu_3Er(\mathbf{L}^{Pr})(NO_3)]^{2+}$, 321.0 $[Cu_3Er(\mathbf{L}^{Pr})]^{3+}$. IR (FT-ATR diamond anvil) $\bar{\nu}/cm^{-1}$ = 1615 (m); 1524 (w); 1461 (m); 1409 (w); 1322 (s); 1257 (m); 1233 (m); 1186 (m); 1095 (m); 1081 (m);1039 (m); 975 (w); 884 (w); 870 (w); 818 (w); 782 (m); 739 (s); 643 (m); 599 (s); 548 (m); 503 (m).

$Cu_3Tm(L^{Pr})(NO_3)_3{\cdot}6H_2O$. Prepared on a 0.05 g of **1** (instead of 0.03 g) scale. Brown powder (0.060 g, 48%). Anal. Calcd for $Cu_3TmC_{33}H_{42}N_9O_{21}$: C, 31.45; H, 3.36; N, 10.00. Found: C, 31.42; H, 3.39; N, 10.38. IR (FT-ATR diamond anvil) $\bar{\nu}/cm^{-1}$ = 1618 (m); 1523 (w); 1458 (m); 1323 (s); 1258 (m); 1233 (m); 1189 (m); 1083 (m);1039 (m); 942 (w); 880 (w); 852 (w); 825 (w); 775 (m); 740 (s); 644 (m); 602 (s); 545 (m); 503 (m).

$Cu_3Yb(L^{Pr})(NO_3)_3{\cdot}4H_2O$. Brown powder (0.030 g, 37%). Anal. Calcd for $Cu_3YbC_{33}H_{30}N_9O_{15}{\cdot}4H_2O$: C, 31.80; H, 3.23; N, 10.11. Found: C, 32.18; H, 3.04; N, 9.88. IR (FT-ATR diamond anvil) $\bar{\nu}/cm^{-1}$ = 1618 (m); 1523 (w); 1458 (m); 1323 (s); 1258 (m); 1233 (m); 1189 (m); 1083 (m); 1039 (m); 974 (w); 880 (w); 852 (w); 825 (w); 775 (m); 740 (s); 643 (m); 599 (s); 545 (m); 503 (m).

RESULTS AND DISCUSSION

Synthesis of the Complexes. In a manner similar to that reported for the Tb^{III} analogue,[20] 3 equiv of $Cu(OAc)_2{\cdot}H_2O$ suspended in a methanol solution of 1 equiv of $Ln(NO_3)_3{\cdot}xH_2O$ (Ln = La, Ce, Pr, Nd, Sm, Eu, Gd, Dy, Ho, Er, Tm, or Yb) was added to a room-temperature solution of 3 equiv of **1** in methanol. After stirring for 2 h, all solids dissolved and a brown solution resulted. Three equivalents of 1,3-diaminopropane in methanol was added dropwise to this solution, resulting in a color change to greenish brown. After stirring for a further hour, diethyl ether was diffused into the reaction solution, resulting in precipitation of a dark green-brown solid. This solid was isolated by filtration, washed with diethyl ether, and dried in vacuo, giving complexes of general formula $Cu_3Ln(\mathbf{L}^{Pr})(NO_3)_3{\cdot}$solvents. Since we observe that the charge-balancing nitrate anions can be involved in the structure in different ways—coordinating to metal ions within the captured coordination complex as well as acting as lattice counterions—it is not possible to be certain of the exact composition of the axial sites of the metal ions for the complexes where single-crystal structure determinations have not been performed. Thus, for all complexes except Ln = Ce, Tb, or Dy, square brackets to indicate the composition of the coordination complex have been omitted from the formulas. With the exception of the crystal structure descriptions, for compactness we will use the informative abbreviation $[Cu_3Ln(\mathbf{L}^{Pr})]$ to refer to these complexes in the following discussion.

Formation of the desired macrocyclic complexes was confirmed by elemental analysis, IR spectroscopy, and ESI-MS. In the IR absorption spectra of the complexes, the C=N stretch of the macrocycle could be seen at 1621 cm^{-1} while no

dx.doi.org/10.1021/ic300819u | Inorg. Chem. 2012, 51, 10603−10612

absorptions for unreacted $H_2\mathbf{L}^1$ (1660 cm^{-1}) or 1,3-diaminopropane (3360 cm^{-1} and 1601 cm^{-1}) were observed. Elemental analysis matched the calculated values expected for complexes of formula $Cu_3Ln(\mathbf{L}^{Pr})(NO_3)_3$·solvents, and peaks corresponding to $[Cu_3Ln(\mathbf{L}^{Pr})(NO_3)_2]^+$, $[Cu_3Ln(\mathbf{L}^{Pr})(NO_3)]^{2+}$, and $[Cu_3Ln(\mathbf{L}^{Pr})]^{3+}$ were seen in all of the ESI-MS spectra. X-ray structure determinations conducted on single crystals of $[Cu_3Ce(\mathbf{L}^{Pr})(NO_3)_3(MeOH)_3]$, $[Cu_3Tb(\mathbf{L}^{Pr})(NO_3)_2(MeOH)_3](NO_3)$,[20] and $[Cu_3Dy(\mathbf{L}^{Pr})(NO_3)_3(MeOH)_3]$ confirmed the success and generality of the template method. IR spectra of the complexes for which a structure determination was not performed were very similar to that of the Tb^{III} analogue.

If $Ln(NO_3)_3·xH_2O$ was not fully dissolved before addition of the metal salts to the solution of **1** or the intermediate was left to stir overnight before addition of the diamine, a brown precipitate would form in the reaction vessel. However, this precipitate gradually redissolves after addition of the amine, and workup proceeds as normal.

Crystal Structures. Single crystals of $[Cu_3Ce(\mathbf{L}^{Pr})(NO_3)_3(MeOH)_3]$ were grown by vapor diffusion of diethyl ether into a solution of the complex in methanol. Structure determination confirmed that the overall structure is similar to the previously reported Tb^{III} analogue.[20] The large Ce^{III} ion is bound in the central O_6 cavity, and the three Cu^{II} ions are bound in the outer N_2O_2 sites (Figure 2, Table 1).

However, there are quite significant differences in the coordination sphere of the Ln^{III}. In contrast to the 9-coordinate Tb^{III} ion (ionic radius = 1.04 Å),[23] the larger Ce^{III} ion (ionic radius =1.14 Å),[23] is 11-coordinate and has a distorted face-capped trigonal prismatic geometry. This coordination sphere is comprised of two nitrate ligands bound in a bidentate fashion on the same face of the macrocycle, one methanol molecule bound on the opposite side of the macrocycle, and the six catecholate donors provided by the macrocycle. The three Cu^{II} ions are all fairly regular square pyramids, slightly distorted toward trigonal bypyramidal (τ for Cu(1) = 0.11, Cu(2) = 0.14, and Cu(3) = 0.06).[24] Bonds to the Cu^{II} ions in $[Cu_3Ce(\mathbf{L}^{Pr})(NO_3)_3(MeOH)_3]$ are similar to the corresponding bonds in the Tb^{III} analogue, indicating that the type of Ln^{III} present does not significantly affect the coordination sphere of the Cu^{II} ions. The apical position of one of the Cu^{II} ions has a weakly coordinated nitrate anion, and the apical positions of the remaining two Cu^{II} ions are occupied by coordinated methanol molecules. The macrocycle adopts a relatively curved conformation. The plane of the second catecholate ring (C13–C18) is oriented 33.52° from the first (C1–C6), and the third (C24–C29) is oriented 30.60° from the second.

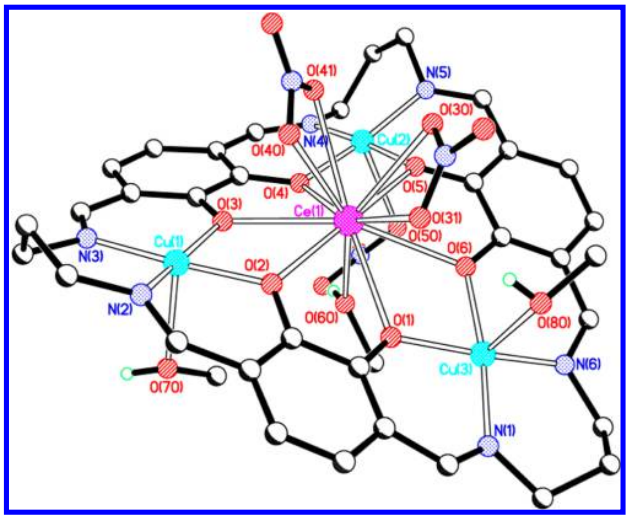

Figure 2. Perspective view of the crystal structure of $[Cu_3Ce(\mathbf{L}^{Pr})(NO_3)_3(MeOH)_3]$. For clarity, nonacidic hydrogen atoms have been omitted. Selected bond lengths (Å): Ce(1)–O(5) 2.487(3); Ce(1)–O2 2.500(3); Ce(1)–O(60) 2.567(3); Ce(1)–O(4) 2.581(3); Ce(1)–O(3) 2.588(3); Ce(1)–O(6) 2.601(3); Ce(1)–O(1) 2.621(3); Ce(1)–O(40) 2.659(3); Ce(1)–O(31) 2.702(3); Ce(1)–O(41) 2.734(4); Ce(1)–O(30) 2.781(4); Cu(1)–O(3) 1.938(3); Cu(1)–O(2) 1.944(3); Cu(1)–N(3) 1.978(4); Cu(1)–N(2) 1.987(4); Cu(1)–O(70) 2.326(3); Cu(2)–O(4) 1.901(3); Cu(2)–O(5) 1.928(3); Cu(2)–N(5) 1.940(4); Cu(2)–N(4) 1.955(4); Cu(3)–O(1) 1.954(3); Cu(3)–O(6) 1.967(3); Cu(3)–N(6) 1.983(4); Cu(3)–N(1) 1.999(4); Cu(3)–O(80) 2.385(3).

The structure of the Dy^{III} analogue is of particular interest given that this 4f ion can produce highly anisotropic effects given the correct environment to optimize its inherent uniaxial anisotropy[9] and because of the SMM behavior observed for the $[Zn_3Dy(\mathbf{L}^{Pr})]$ analogue in a dc field.[8a] Single crystals of $[Cu_3Dy(\mathbf{L}^{Pr})(NO_3)_3(MeOH)_3]$ were grown by vapor diffusion of diethyl ether into a solution of the complex in methanol. The overall structure (Figure 3, Table 1) is similar to the Ce^{III} and Tb^{III} analogues, but, as outlined above, the differences in the details are of paramount interest in performing this systematic study. In contrast to the 11-coordinate Ce^{III} ion, but like the similarly sized Tb^{III} ion,[20] the Dy^{III} ion (ionic radius =1.03 Å),[23] is 9-coordinate and has a distorted tricapped trigonal prismatic geometry. As with the other two complexes, the Cu^{II} ions in the Dy^{III} complex all have regular square pyramidal geometries (τ for Cu(1) = 0.03, Cu(2) = 0.16, and Cu(3) = 0.06; for the major occupancy NO_3 and MeOH positions). The Cu(1) ion also forms a second axial interaction; however, it is very weak (Cu(1)···O(40) = 3.129 Å), so it is best considered to be 5 coordinate. Only one nitrate anion is coordinated to the Dy^{III}; the second is coordinated in the apical position of a Cu^{II} ion, and the third is very weakly interacting with the second axial site of Cu(2), as already mentioned. One methanol molecule is coordinated to the Dy^{III} ion, and the remaining two are each coordinated to a Cu^{II} ion. The curvature of the macrocycle is similar to that of the Ce^{III} analogue, with comparable angles between the planes formed by the successive catecholate rings (33.52° and 30.60° for $[Cu_3Ce(\mathbf{L}^{Pr})(NO_3)_3(MeOH)_3]$ versus 34.97° and 27.41° for $[Cu_3Dy(\mathbf{L}^{Pr})(NO_3)_3(MeOH)_3]$).

Magnetic Properties. The temperature dependence of χT for the complexes gave, in each case, a room-temperature χT value consistent with the expected value for three Cu^{II} ions and the relevant Ln^{III} ion (Table 1 and Figure 4). The temperature dependence of χT was measured down to 1.8 K. However, it is not trivial to determine the relative contribution to these thermal behaviors of either the 3d–3d/3d–4f magnetic interactions or the spin–orbit coupling of the lanthanide ion.

We have previously shown for $[Cu_3La(\mathbf{L}^{Pr})]$ that the Cu^{II}–Cu^{II} interaction is weakly ferromagnetic (J/k_B = +0.5(1) K).[20] In the case of Ln = Ce^{III}, Pr^{III}, Nd^{III}, and Yb^{III}, the χT value decreases steadily from 300 K to a minimum at 1.8 K that is lower than the value for the La^{III} analogue (1.51 cm^3 K mol^{-1}). This result suggests antiferromagnetic interaction is present between the Cu^{II} and the Ln^{III} ions for those complexes. For $[Cu_3Sm(\mathbf{L}^{Pr})]$ and $[Cu_3Eu(\mathbf{L}^{Pr})]$, the Ln^{III} ion is quasi-diamagnetic and as a result the χT value at 1.8 K is close to

dx.doi.org/10.1021/ic300819u | Inorg. Chem. 2012, 51, 10603–10612

Table 1. Comparison of the Structural Parameters of the $Cu_3Ln(L^{Pr})(NO_3)_3 \cdot x$solvents Complexes (Ln = Ce, Tb, or Dy)

distance (Å) or angle (deg)	$[Cu_3Ce(L^{Pr})(NO_3)_3(MeOH)_3]$	$[Cu_3Tb(L^{Pr})(NO_3)_2(MeOH)_3](NO_3)$[20]	$[Cu_3Dy(L^{Pr})(NO_3)_3(MeOH)_3]$
$Ln-O_{catecholate}$ range (average)	2.487–2.621 (2.563)	2.407–2.464 (2.439)	2.402–2.464 (2.429)
$Ln-O_{methanol}$	2.567	2.300	2.297
$Ln-O_{nitrate}$ range (average)	2.659–2.781 (2.719)	2.484–2.513 (2.499)	2.460–2.485 (2.473)
$Cu-O_{catecholate}$ range (average)	1.901–1.967 (1.939)	1.915–1.944 (1.927)	1.916–1.948 (1.931)
$Cu-N_{imine}$ range (average)	1.940–1.999 (1.974)	1.951–1.985 (1.972)	1.952–1.974 (1.967)
$Cu-O_{methanol}$ range (average)	2.326–2.385 (2.356)	2.324–2.534 (2.429)	2.319–2.513 (2.416)
$Cu-O_{nitrate}$	2.474	2.494	2.446
Cu–O–Ln range (average)	106.9–111.7 (109.9)	109.7–112.2 (110.9)	109.4–111.7 (110.7)
Cu···Cu range (average)	6.179–6.361 (6.280)	6.108–6.331 (6.244)	6.066–6.271 (6.220)
Cu···Ln range (average)	3.623–3.797 (3.703)	3.585–3.636 (3.610)	3.571–3.624 (3.599)
shortest Ln···Ln in lattice	9.92	8.59	9.85

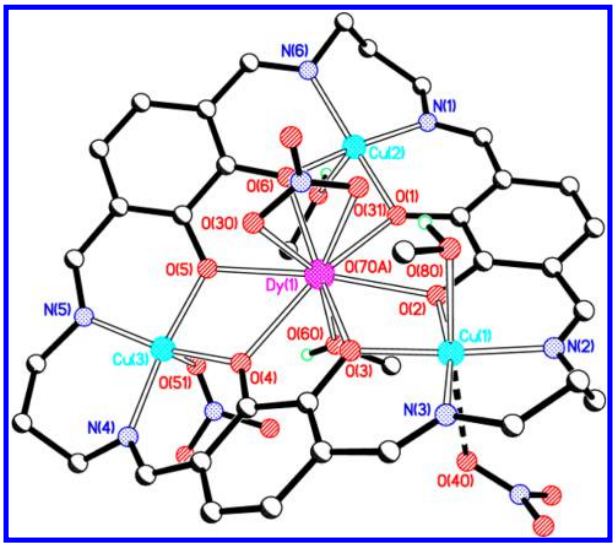

Figure 3. Perspective view of the crystal structure of $[Cu_3Dy(L^{Pr})(NO_3)_3(MeOH)_3]$. For clarity, nonacidic hydrogen atoms and the minor components of disordered atoms have been omitted. Weak Cu(1)···O(40) interaction is indicated with a dotted line. Selected bond lengths (Å): Dy(1)–O(60) 2.297(4); Dy(1)–O(3) 2.402(4); Dy(1)–O(6) 2.413(4); Dy(1)–O(1) 2.425(4); Dy(1)–O(4) 2.430(4); Dy(1)–O(2) 2.440(4); Dy(1)–O(30) 2.460(4); Dy(1)–O(5) 2.464(4); Dy(1)–O(31) 2.485(4); Dy(1)–N(30) 2.885(5); Cu(1)–O(2) 1.931(4); Cu(1)–O(3) 1.948(4); Cu(1)–N(3) 1.973(6); Cu(1)–N(2) 1.974(6); Cu(1)–O(45) 2.441(17); Cu(1)–O(80) 2.513(5); Cu(1)–O(40) 3.129(13); Cu(2)–O(6) 1.920(4); Cu(2)–O(1) 1.938(4); Cu(2)–N(1) 1.952(6); Cu(2)–N(6) 1.974(6); Cu(2)–O(70B) 2.31(3); Cu(2)–O(70A) 2.319(10); Cu(3)–O(5) 1.916(4); Cu(3)–O(4) 1.935(4); Cu(3)–N(5) 1.963(6); Cu(3)–N(4) 1.965(7); Cu(3)–O(51) 2.446(8); Cu(3)–O(57) 2.664(15).

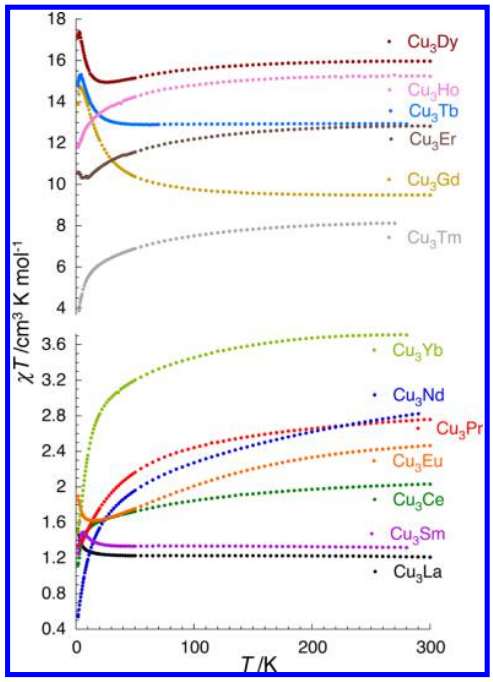

Figure 4. Temperature dependence of χT product (with χ defined as the molar magnetic susceptibility at 1000 Oe and equal to M/H per mole of complex) for complexes $Cu_3Ln(L^{Pr})(NO_3)_3 \cdot x$solvents, where Ln = La, Ce, Pr, Nd, Sm, Eu, Gd, Tb, Dy, Ho, Er, Tm, or Yb.

the value for the La^{III} analogue. In the case of $[Cu_3Gd(L^{Pr})]$, which contains an isotropic Gd^{III} ion, the contribution of spin–orbit coupling can be excluded and so the steady increase to a maximum at 1.8 K unambiguously shows that the Cu^{II}–Gd^{III} interaction is ferromagnetic (vide infra). For $[Cu_3Tb(L^{Pr})]$ and $[Cu_3Dy(L^{Pr})]$ it can also be demonstrated that the Cu^{II}–Ln^{III} interaction is ferromagnetic (ab initio calculations, see below).

Complexes were checked for SMM behavior by investigation of their magnetic properties using dc and ac fields, Table 2. The field dependence of the magnetization showed a complete absence of hysteresis effect even at the lowest temperature limit of the measurement (1.8 K, Figure S1, Supporting Information). The field dependence of the *reduced* magnetization (Figure S2, Supporting Information) for the complexes showed that in the case of Ln = Gd^{III} and Eu^{III} the curves could be superposed on a single master curve as expected for an isotropic system with a well-defined ground state. This is not the case for any of the other complexes, indicating the presence of magnetic anisotropy or low-lying excited states. The lack of SMM behavior was further underscored by measuring the ac susceptibility; none of the new $Cu_3Ln(L^{Pr})(NO_3)_3 \cdot$solvents complexes (Ln = Ce, Pr, Nd, Sm, Eu, Gd, Dy, Ho, Er, Tm, or Yb) exhibited an out-of-phase component. Only frequency-independent in-phase components were observed, indicating that there is no significant barrier (in comparison to the thermal energy) to spin reversal present in any of the complexes. As we reported previously, the Tb^{III} complex, $[Cu_3Tb(L^{Pr})]$, shows SMM properties.[20] Although this complex exhibited a frequency-dependent out-of-phase component to ac susceptibility, the position of the maximum χ'' could not be determined within the experimental limit of the measurement. This precluded determination of the thermal

dx.doi.org/10.1021/ic300819u | Inorg. Chem. 2012, 51, 10603–10612

Table 2. Magnetic Properties of the $Cu_3Ln(L^{Pr})(NO_3)_3{\cdot}x$solvents Complexes with Ln = La, Ce, Pr, Nd, Sm, Eu, Gd, Tb, Dy, Ho, Er, Tm, or Yb

complex	ground spin state of Ln^{III} ion	measured/expected (with g_{Cu} = 2) χT at 300 K (cm^3 K mol^{-1})	χT at 1.8 K (cm^3 K mol^{-1})	M at 1.8 K and 70 kOe (μ_B)	SMM
$Cu_3La(L^{Pr})(NO_3)_3{\cdot}3MeOH{\cdot}H_2O$	$^1S_0$	1.20/1.13	1.51	2.97	no
$[Cu_3Ce(L^{Pr})(NO_3)_3(MeOH)_2(H_2O)]{\cdot}H_2O$	$^2F_{5/2}$	2.03/1.93	1.12	3.50	no
$Cu_3Pr(L^{Pr})(NO_3)_3{\cdot}MeOH{\cdot}4H_2O$	$^3H_4$	2.76/2.73	1.3	3.35	no
$Cu_3Nd(L^{Pr})(NO_3)_3{\cdot}5H_2O$	$^4I_{9/2}$	2.82/2.77	0.54	2.05	no
$Cu_3Sm(L^{Pr})(NO3)_3{\cdot}MeOH{\cdot}2H_2O$	$^6H_{5/2}$	1.32/1.22	1.26	2.59	no
$Cu_3Eu(L^{Pr})(NO_3)_3{\cdot}MeOH{\cdot}3H_2O$	$^7F_0$	2.46/2.53	1.90	3.26	no
$Cu_3Gd(L^{Pr})(NO_3)_3{\cdot}MeOH{\cdot}3H_2O$	$^8S_{7/2}$	9.63/9.00	13.88	10.15	no
$[Cu_3Tb(L^{Pr})(NO_3)_2(MeOH)(H_2O)_2](NO_3){\cdot}3H_2O$	$^7F_6$	12.93/12.94	14.78	7.97	yes[20]
$[Cu_3Dy(L^{Pr})(NO_3)_3(MeOH)_3]{\cdot}3H_2O$	$^6H_{15/2}$	15.97/15.29	17.13	8.58	no
$Cu_3Ho(L^{Pr})(NO_3)_3{\cdot}MeOH{\cdot}3H_2O$	$^5I_8$	15.24/15.19	11.80	9.17	no
$Cu_3Er(L^{Pr})(NO_3)_3{\cdot}MeOH{\cdot}3H_2O$	$^4I_{15/2}$	12.82/12.60	10.59	8.89	no
$Cu_3Tm(L^{Pr})(NO_3)_3{\cdot}6H_2O$	$^3H_6$	8.12/8.28	3.55	5.85	no
$Cu_3Yb(L^{Pr})(NO_3)_3{\cdot}4H_2O$	$^2F_{7/2}$	3.71/3.70	1.49	3.69	no

dependence of the relaxation time and thus an estimation of the SMM energy barrier.

In most of these complexes, it is difficult to quantify the magnetic interactions between the S = 1/2 Cu^{II} spins and the magnetic Ln^{III} centers due to the intrinsic magnetism of the Ln^{III} ions. However, the $[Cu_3Gd(L^{Pr})]$ complex contains only isotropic metal ions, so it was possible to model the temperature dependence of the magnetic susceptibility and thus to extract the Cu^{II}–Gd^{III} and Cu^{II}–Cu^{II} interactions. As a first approximation, a simple symmetrical triangular model was used (Figure S3, Supporting Information). In keeping with the structural motif, the Heisenberg spin Hamiltonian can be written as follows

$$\mathbf{H} = -2J_{Cu-Cu}\{\mathbf{S}_2{\cdot}\mathbf{S}_3 + \mathbf{S}_3{\cdot}\mathbf{S}_4 + \mathbf{S}_2{\cdot}\mathbf{S}_4\} - 2J_{Cu-Ln}\mathbf{S}_1 \cdot\{\mathbf{S}_2 + \mathbf{S}_3 + \mathbf{S}_4\} \quad (1)$$

where J_{Cu-Cu} represents the average exchange interaction between adjacent Cu^{II} centers, J_{Cu-Ln} represents the Cu^{II}–Gd^{III} exchange interaction, and S_i are the spin operators with S_2 = S_3 = S_4 = 1/2 for Cu^{II} and S_1 = 7/2 for Gd^{III}.

Full diagonalization of the spin Hamiltonian and calculation of the magnetic susceptibility were performed using the Magpack program.[25] In order to reproduce the decrease of the χT product below 3.9 K, intercomplex interactions were included in the frame of the mean field approximation so that the magnetic susceptibility expression becomes

$$\chi = \frac{\chi_{[Cu_3Ln]}}{1 - \frac{2zJ'}{Ng_{av}^2\mu_B^2}\chi_{[Cu_3Ln]}} \quad (2)$$

Here J' is the intercomplex interaction and z the number of neighboring complexes. As shown in Figure 5, an excellent simulation of the experimental χT vs T and M vs H/T data down to 1.8 K is obtained using this model, with J_{Cu-Cu}/k_B = +0.51(2) K, J_{Cu-Gd}/k_B = +2.5(1) K, g_{av} = 2.03(5), and zJ'/k_B = −0.011(1) K. This result confirms the presence of ferromagnetic coupling between the S = 1/2 Cu^{II} spins (similar to those observed in $[Cu_3La(L^{Pr})]$; J_{Cu-Cu}/k_B= +0.5(1) K)[20] and between the S = 1/2 Cu^{II} and S = 7/2 Gd^{III} spins, leading to an S_T = 5 spin ground state for $[Cu_3Gd(L^{Pr})]$.

Ab Initio Calculations. Having previously reported[20] the magnetic properties of $[Cu_3Tb(L^{Pr})(NO_3)_2(MeOH)(H_2O)_2]$-$(NO_3){\cdot}3H_2O$ and $Cu_3La(L^{Pr})(NO_3)_3{\cdot}3MeOH{\cdot}H_2O$, we now present a detailed computational analysis of these complexes as well as the newly synthesized $[Cu_3Dy(L^{Pr})(NO_3)_3(MeOH)_3]$ complex. High-level ab initio calculations using MOLCAS 7.6[26] were performed on individual metal fragments, while the exchange interaction between magnetic centers was simulated within the Lines model[27] using POLY_ANISO.[28] The exchange interaction between magnetic ions was computed on the basis of the lowest states obtained from the ab initio calculation for each magnetic site. As a result, the total exchange basis for $[Cu_3La(L^{Pr})]$, $[Cu_3Tb(L^{Pr})]$, and $[Cu_3Dy(L^{Pr})]$ contains 2^3 = 8, 13 × 2^3 = 104, and 16 × 2^3 = 128 functions, respectively. One La^{III} ion has $2J$ + 1 functions; three Cu^{II} ions have $(2S + 1)^3$ functions; hence, each complex has a total of $(2J + 1) \times (2S + 1)^3$ functions. The magnetic contribution of the higher excited states was added via second-order perturbation theory. Due to the fact that the structure of the $[Cu_3La(L^{Pr})]$ complex was not available, its magnetic properties were computed using the data of the structurally characterized $[Cu_3Tb(L^{Pr})]$ complex, substituting Tb^{III} with La^{III} (Figure S4, Supporting Information).

Results of the ab initio calculations reveal a strong axial anisotropy on the Tb^{III} ion (Figure 6 and Tables 3 and 4) and Dy^{III} ion (Figure 7 and Table 4). Cu^{II} ions show typical minor

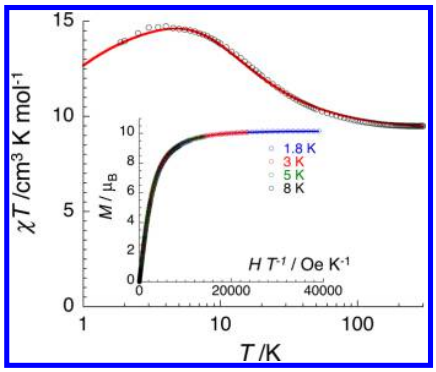

Figure 5. Comparison between measured (empty dots) and theoretical (red line, see text) temperature dependence of χT for $[Cu_3Gd(L^{Pr})]$ (shown in the semilogarithmic plot, with χ defined as molar magnetic susceptibility at 1000 Oe and equal to M/H per mole of complex). (Inset) Experimental (open dots) and theoretical (solid lines; see text) field dependence of the magnetization for $[Cu_3Gd(L^{Pr})]$ at different temperatures.

dx.doi.org/10.1021/ic300819u | Inorg. Chem. 2012, 51, 10603−10612

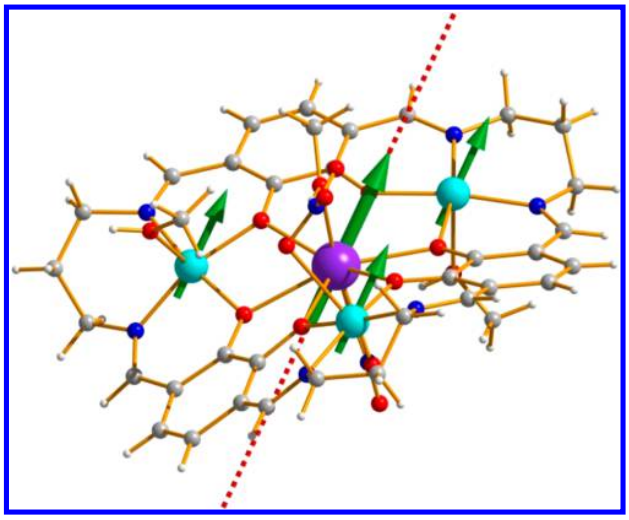

Figure 6. Orientation of the local magnetic moments in the ground state of $[Cu_3Tb(L^{Pr})(NO_3)_2(MeOH)_3](NO_3)$ (green arrows) and orientation of the anisotropic axis of the Tb^{III} ion (red dotted line; at 46.08° to Cu_3 plane).

Table 3. Calculated Energies (cm^{-1}) of Local Spin−Orbit Singlets on Tb^{III} in $[Cu_3Tb(L^{Pr})(NO_3)_2(MeOH)_3](NO_3)$ and Kramers Doublets on Dy^{III} and Cu^{II} Fragments in $[Cu_3Dy(L^{Pr})(NO_3)_3(MeOH)_3]$

Tb	Dy	Cu(1)	Cu(2)	Cu(3)
0	0	0	0	0
4.2	47	21 077	18 893	23 684
59	82	24 372	19 776	25 930
91	219	25 821	22 841	27 751
102	228	28 466	23 975	28 491
153	286	29 452	40 036	29 858
164	320	36 519	40 476	34 803
211	435	38 565	44 961	42 487
220		39 951	46 591	43 585
264		41 054	57 589	46 601
267		45 936	62 201	47 797
472		50 552	63 165	49 330
472				
2143				

Table 4. Local *g* Tensors of the Ground Ising Doublet of the Tb^{III} Ion in $[Cu_3Tb(L^{Pr})(NO_3)_2(MeOH)_3](NO_3)$ and Ground Kramers Doublet of the Dy^{III} and Cu^{II} Ions in $[Cu_3Dy(L^{Pr})(NO_3)_3(MeOH)_3]$

	Tb	Dy	Cu(1)	Cu(2)	Cu(3)
g_x	0	0.033	2.041	2.045	2.040
g_y	0	0.055	2.044	2.056	2.044
g_z	16.451	18.571	2.184	2.229	2.176
$\sqrt{\frac{(g_x^2+g_y^2+g_z^2)}{3}}$	9.49	10.72	2.091	2.112	2.088

anisotropy for a square-pyramidal geometry (see Supporting Information for computational details). Simulations of the magnetic properties of $[Cu_3La(L^{Pr})]$ were best reproduced by exchange parameter J_{Cu-Cu}/k_B= +0.57 K, which is quite close to the purely isotropic fit reported in ref 20 (J_{Cu-Cu}/k_B= 0.5(1) K), confirming the fact that the magnetic anisotropy on Cu^{II} ions is not important. The averaged *g* values for the Cu^{II} sites in

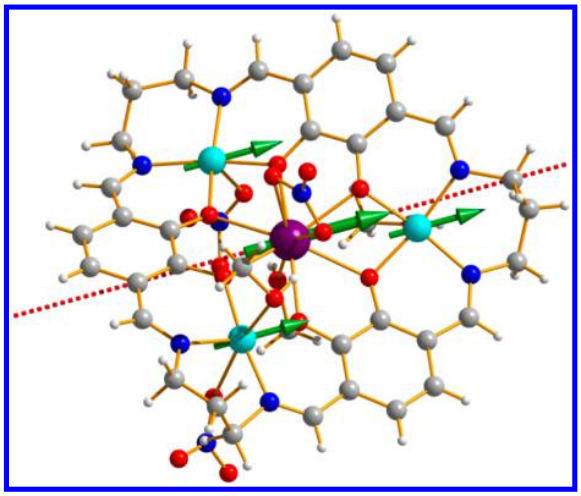

Figure 7. Orientation of local magnetic moments in the ground state of $[Cu_3Dy(L^{Pr})(NO_3)_3(MeOH)_3]$ (green arrows) and orientation of the anisotropic axis of the Dy^{III} ion (red dotted line; at 2.22° to Cu_3 plane).

$[Cu_3Tb(L^{Pr})]$ (Table 4) are close to the isotropic value (2.08(2)) obtained for $[Cu_3La(L^{Pr})]$,[20] which means that the magnetic properties of the Cu^{II} ions are not influenced strongly by the nature of the lanthanide ion.

The magnetic properties of $[Cu_3Tb(L^{Pr})]$ are best described by the Lines exchange parameters J_{Tb-Cu}/k_B = +4.14 K and J_{Cu-Cu}/k_B = +1.41 K, while the magnetic properties of $[Cu_3Dy(L^{Pr})]$ are best described by J_{Dy-Cu}/k_B = +3.74 K and J_{Cu-Cu}/k_B = +0.86 K (Figure 8). The small difference in the magnitude of J_{Cu-Cu} is due to subtle geometric differences in the Cu^{II}−catecholate−Cu^{II} moiety.

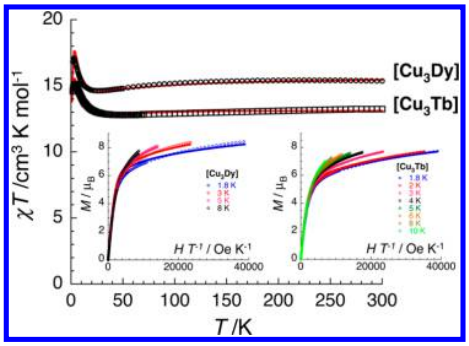

Figure 8. Comparison between measured (empty symbols) and ab initio calculated (solid lines) temperature dependence of χT for $[Cu_3Dy(L^{Pr})(NO_3)_3(MeOH)_3]$ and $[Cu_3Tb(L^{Pr})(NO_3)_2(MeOH)_3](NO_3)$ (with χ defined as molar magnetic susceptibility at 1000 Oe and equal to *M*/*H* per mole of complex). (Inset) Experimental (open symbols) and ab initio calculated (solid lines) field dependence of the magnetization for $[Cu_3Dy(L^{Pr})(NO_3)_3(MeOH)_3]$ and $[Cu_3Tb(L^{Pr})(NO_3)_2(MeOH)_3](NO_3)$ at different temperatures.

It is difficult to speculate on why the Cu^{II}−Cu^{II} interaction in these compounds is ferromagnetic and not antiferromagnetic, but it is weak as expected given that (a) it involves a four-atom bridge and (b) in related studies the magnetic properties of complexes with a similar Cu^{II}−catecholate−Cu^{II} moiety have been successfully simulated by assuming the Cu^{II}−Cu^{II} interaction across the four-atom catecholate bridge is

dx.doi.org/10.1021/ic300819u | Inorg. Chem. 2012, 51, 10603−10612

negligible.[29] In order to gain insight into the Cu^{II}−Cu^{II} exchange interaction, broken-symmetry density functional theory (BS-DFT) calculations[33] were performed on [Cu_3Tb(L^{Pr})], with the experimentally observed geometry and the Tb(III) ion substituted by the nonmagnetic La(III) ion. Calculations were carried out within ORCA[34] using the B3LYP functional and SVP basis set. Four calculations were done, one for projection of the total spin M = 3/2, corresponding to spin-up projections of the local S = 1/2 on three Cu(II) sites, and three calculations for the total spin projection M = 1/2, corresponding to flipping of one spin down on each of the three copper sites, respectively. Then the exchange coupling constants were calculated using the generalized spin projection method,[35] giving the following values: $J_{Cu1-Cu2}/k_B$ = +2.8 × 10^{-4} K, $J_{Cu2-Cu3}/k_B$ = +4.4 K, and $J_{Cu1-Cu3}/k_B$ = +0.64 K. Although all are ferromagnetic (as also derived from the fitting of the magnetic data), the three exchange parameters differ drastically in magnitude. The reason is small deviations of the geometry of the macrocycle from an ideal trigonal symmetry (Figure 3). However, the average value of these parameters, $J_{average}/k_B$ = +1.7 K, is close to the value J_{Cu-Cu}/k_B = +1.41 K obtained from the fitting of magnetic data for [Cu_3Tb(L^{Pr})] (Figure 8).

Further insight is obtained from analysis of magnetic orbitals on the Cu(II) sites. Making a localization transformation of the three singly occupied molecular orbitals obtained in the high-spin (M = 3/2) calculation, the localized magnetic (Anderson's) orbitals on the copper sites are obtained (Figure 9). This shows that the orbitals localized at sites Cu2 and Cu3 do not show delocalization on the mutual ion and its closest environment, which explains why the strongest ferromagnetic coupling is obtained for this pair. In the Cu1−Cu3 pair there is a non-negligible delocalization on the mutual copper ion (Figure 9a and 9c), which however does not lead to antiferromagnetic coupling due to a compensating effect of (ferromagnetic) potential exchange contribution.[36] On the other hand, the exchange contribution from the spin polarization of the ligand (here the entire macrocycle), which is generally expected to be strong for a conjugated ligand,[37] seems to be of less importance in the present case. Indeed, the conjugated path O−C−C−O connecting two Cu(II) ions (Figure 9) favors antiferromagnetic coupling via a spin polarization mechanism, while the overall ferromagnetic coupling obtained for all copper pairs suggests that this mechanism is, at least, not stronger than the direct ferromagnetic exchange interaction. The latter is already weak due to the relatively large Cu−Cu distances. We may conclude that the small values of exchange parameters obtained are the result of strong compensation of ferro- and antiferromagnetic interactions for Cu−Cu pairs. In support of this picture, the calculated exchange parameters for [Cu_3Ce(L^{Pr})], using the same approach and replacing Ce(III) by La(III) while keeping the experimental geometry intact, gave $J_{Cu1-Cu2}/k_B$ = +3.2 × 10^{-3} K, $J_{Cu2-Cu3}/k_B$ = +0.38 K, and $J_{Cu1-Cu3}/k_B$ = −3.8 K (the localized magnetic orbitals are shown in Figure S5, Supporting Information). The preponderant antiferromagnetic exchange in this compound results from small structural changes of the macrocycle compared to [Cu_3Tb(L^{Pr})] which push the balance of the three exchange contributions from ferro- to antiferromagnetic.

It is worth noting that the axis of anisotropy for the Dy^{III} ion is at 2.22° (similar to the 5.05° found in the [Zn_3Dy(L^{Pr})] analogue),[8a] and for the Tb^{III} ion it is at 46.08°, from the plane formed by the three Cu^{II} ions (Figures 6 and 7).

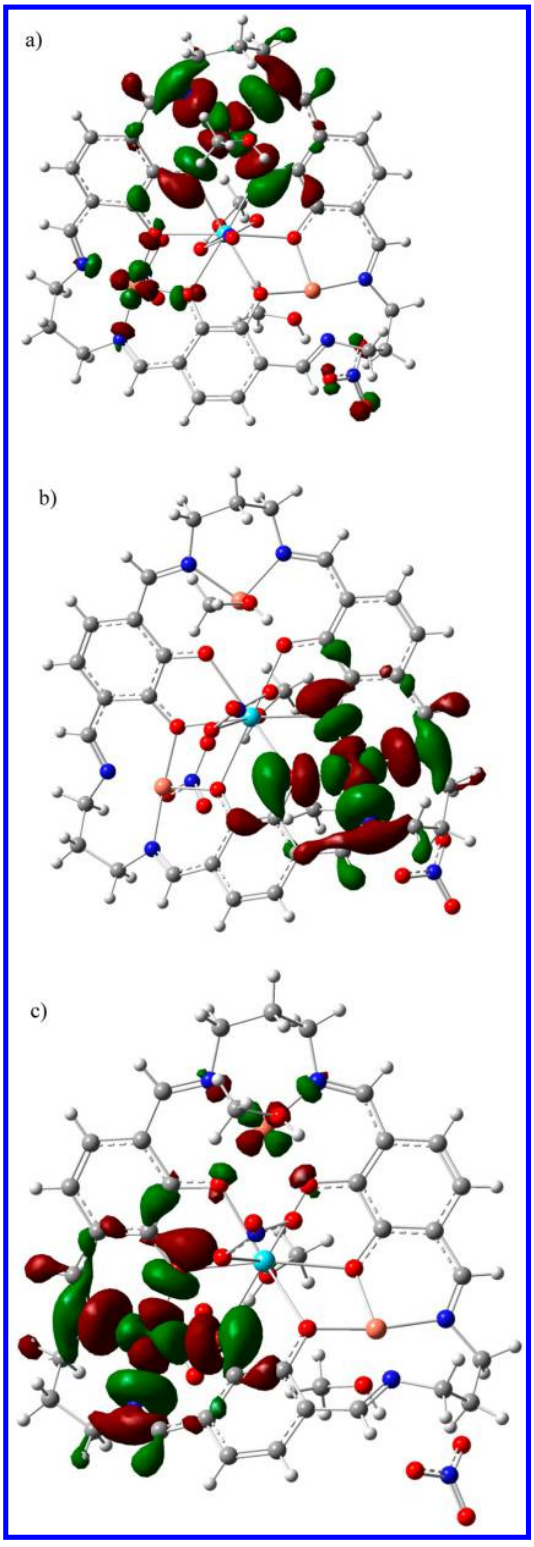

Figure 9. Localized magnetic orbitals on Cu1 (a), Cu2 (b), and Cu3 (c) in compound [Cu_3Tb(L^{Pr})(NO_3)$_2$($MeOH$)$_3$](NO_3). See text for details.

The reason for relatively fast relaxation of magnetization in [Cu_3Tb(L^{Pr})] is the deviation from axiality of the ground

dx.doi.org/10.1021/ic300819u | Inorg. Chem. 2012, 51, 10603−10612

exchange Kramers doublet. The relatively large perpendicular components (g_X = 0.070 and g_Y = 0.085, Table 5) are the reason for quantum tunneling induced by magnetic fields perpendicular to the main anisotropy axis (which coincides with the anisotropy axis on Tb^{III}, see Figure 6) of the ground Kramers doublet.

Table 5. Energies of the Lowest Four Exchange Doublets (cm^{-1}) and Molecular *g* Tensors for the Ground Exchange Doublets for Complexes $[Cu_3Tb(L^{Pr})(NO_3)_2(MeOH)_3](NO_3)$, $[Cu_3La(L^{Pr})]$, and $[Cu_3Dy(L^{Pr})(NO_3)_3(MeOH)_3]$

$[Cu_3Tb(L^{Pr})(NO_3)_2(MeOH)_3](NO_3)$	$Cu_3La(L^{Pr})(NO_3)_3$	$[Cu_3Dy(L^{Pr})(NO_3)_3(MeOH)_3]$
0.0000000	0.0000000	0.0000000
0.0000000	0.0000000	0.0000163
7.1058319	0.0012663	5.9538112
7.1058320	0.0012663	5.9603006
9.0643506	0.8823092	7.0177245
9.0643507	0.8823092	7.0215063
9.0685331	0.8828293	7.0234860
9.0685332	0.8828293	7.0272403
g tensor of the ground exchange doublet		
g_X = 0.070	g_X = 0.213	g_X = 0.000
g_Y = 0.085	g_Y = 0.222	g_Y = 0.000
g_Z = 22.580	g_Z = 6.508	g_Z = 24.917

A similar situation has been found in the recently investigated $[Zn_3Dy(L^{Pr})]$ complex,[8a] where the perpendicular components of the *g* tensor were found to be of the same order of magnitude as in $[Cu_3Tb(L^{Pr})]$, although a maximum in the frequency dependence of χ'' was not observed until a dc magnetic field of 1000 Oe was applied. We note that similar magnetic behavior was also reported recently for a $[Co^{II}_3Co^{III}_4]$ complex,[30] where the ground exchange Kramers doublet also showed marked departure from a perfect axiality. The SMM properties of $[Cu_3Tb(L^{Pr})]$ could potentially be enhanced if the splitting between the lowest two levels of Tb^{III} ion (4.2 cm^{-1}/6.04 K) could be diminished by varying the nearest environment of the ion. A recent example of this kind is the family of $[Tb_3]$ SMMs for which ab initio calculations determined the splitting of the lowest levels of the Tb^{III} ions at 0.03−0.13 cm^{-1} (0.04−0.19 K).[31]

Having prepared the $[Zn_3Dy(L^{Pr})]$ SMM,[8a] we investigated why the analogous Cu^{II} complex, $[Cu_3Dy(L^{Pr})]$, did not display any slow relaxation of its magnetization. In contrast to the Kramers system $[Zn_3Dy(L^{Pr})]$, the complex $[Cu_3Dy(LPr)]$ is an Ising system with the transverse molecular g factors (g_X and g_Y) inherently equal to zero. In this case, the tunnelling splitting is obtained from the energy difference between the two components of the ground exchange doublet. For Kramers systems, however, the tunnelling splitting is proportional to the transverse components of the *g* tensor of the ground Kramers doublet and appears mainly as a result of the presence of perpendicular magnetic fields. For $[Cu_3Dy(L^{Pr})]$, the tunnel splitting is $\sim 1.6 \times 10^{-5}$ cm^{-1} (2.3×10^{-5} K; Table 5), which is quite large compared to other well-known SMMs. This large tunnel splitting results in a rapid quantum tunnelling relaxation time induced by magnetic fields and the absence of an out-of-phase component in zero dc field. The deviation from axiality of the central Dy^{III} ion in $[Cu_3Dy(L^{Pr})]$ is similar to but presumably somewhat less than that of the Dy^{III} ion in $[Zn_3Dy(L^{Pr})]$, where g_X = 0.10 and g_Y = 0.25. Thus, observation of a weak out-of-phase component in the absence of a dc field is possible for $[Zn_3Dy(L^{Pr})]$, while this is not the case for $[Cu_3Dy(L^{Pr})]$. The deviation from axiality in $[Zn_3Dy(L^{Pr})]$ and $[Cu_3Dy(L^{Pr})]$ and the relatively large splitting on the Tb^{III} ion in $[Cu_3Tb(L^{Pr})]$ are due to the low-symmetry components of the ligand field of comparable strength. Once again, our investigations suggest that perfect magnetic axiality (i.e., $g_X = g_Y = 0$ for the Kramers complexes; zero tunnel splitting for the Ising complexes) is the key for obtaining SMMs with higher energy barriers to blocking of magnetization.

CONCLUSIONS

We prepared a family of 13 tetranuclear Cu^{II}−Ln^{III} complexes of the macrocycle $(L^{Pr})^{6-}$. The use of a carefully designed, large, multiple-binding-pocket, organic macrocycle provides the desired control of nuclearity and structure, generating this large family of complexes with very similar overall structures. One complex, $[Cu_3Tb(L^{Pr})]$, displayed magnetic properties indicative of SMM behavior. However, none of the other complexes displayed such behavior. This was surprising in the case of $[Cu_3Dy(L^{Pr})]$, as the Zn^{II} analogue was earlier shown to display slow relaxation of magnetization under a dc field, so simplistically one might anticipate that replacement of the $S = 0$ Zn^{II} ions by $S = 1/2$ Cu^{II} ions might "improve" the SMM behavior. However, the ab initio calculations show that the reason the Cu^{II} analogue is not a SMM is a result of deviation from perfect magnetic axiality, which in turn results from the low symmetry of the ligand field. In order to better understand and improve SMM behavior, further effort must go into establishing under what conditions high magnetic axiality can be achieved. A remarkable feature of lanthanide complexes is that comparably high axiality can be achieved in low-symmetry and slightly distorted high-symmetry complexes.[32] We are now looking to replace the Cu^{II} ions with other paramagnetic centers in order to explore which blends of 3d and 4f ions provide stronger magnetic anisotropy and hence optimize SMM behavior. Furthermore, we intend to devise modified macrocyclic systems in order to control the magnetic axiality of these Zn_3Ln and Cu_3Ln complexes. In summary, we are now extending this systematic approach, offered by the combination of large, carefully tailored macrocyclic ligands and selected blends of 3d−4f ions, to target production of enclosed, stable, and soluble $[M_3Ln]$ coordination complexes with improved SMM properties.

ASSOCIATED CONTENT

Supporting Information

Additional magnetic data for the complexes, and further details of the theoretical analysis. This material is available free of charge via the Internet at http://pubs.acs.org.

AUTHOR INFORMATION

Corresponding Author

*E-mail: clerac@crpp-bordeaux.cnrs.fr (R.C.); Liviu.Chibotaru@chem.kuleuven.be (L.C.); annie.powell@kit.edu (A.K.P.); sbrooker@chemistry.otago.ac.nz (S.B.).

Notes

The authors declare no competing financial interest.

■ ACKNOWLEDGMENTS

This work was supported by grants from the University of Otago (including a Ph.D. scholarship for H.L.C.F.) and the MacDiarmid Institute for Advanced Materials and Nanotechnology. We also thank the University of Bordeaux, the CNRS, the Région Aquitaine (GIS Advanced Materials in Aquitaine and the COMET Project), the Dumont d'Urville NZ-France Science & Technology Support Programme (No. 23793PH), the Julius von Haast Fellowship Fund (RSNZ), and the Flemish Science Foundation (FWO, including a postdoctoral fellowship to L.U.) for financial support.

■ REFERENCES

(1) (a) Gatteschi, D.; Sessoli, R. *Angew. Chem., Int. Ed.* **2003**, *42*, 268. (b) Gatteschi, D.; Sessoli, R.; Villain, F. *Molecular Nanomagnets*; Oxford University Press: Oxford, 2006.
(2) Wernsdorfer, W. *Int. J. Nanotechnol.* **2010**, *7*, 497.
(3) Rinehart, J. D.; Fang, M.; Evans, W. J.; Long, J. R. *Nat. Chem.* **2011**, *3*, 538.
(4) Aromí, G.; Brechin, E. K. *Struct. Bonding (Berlin)* **2006**, 1.
(5) (a) Sessoli, R.; Powell, A. K. *Coord. Chem. Rev.* **2009**, *253*, 2328. (b) Kostakis, G. E.; Hewitt, I. J.; Ako, A. M.; Mereacre, V.; Powell, A. K. *Philos. Trans. R. Soc. London, Ser. A* **2010**, *368*, 1509.
(6) Andruh, M.; Costes, J.-P.; Diaz, C.; Gao, S. *Inorg. Chem.* **2009**, *48*, 3342.
(7) Winpenny, R. E. P. *J. Chem. Soc., Dalton Trans.* **2002**, 1.
(8) (a) Feltham, H. L. C.; Lan, Y.; Klöwer, F.; Ungur, L.; Chibotaru, L. F.; Powell, A. K.; Brooker, S. *Chem.—Eur. J.* **2011**, *17*, 4362. (b) Guo, Y.-N.; Xu, G.-F.; Wernsdorfer, W.; Ungur, L.; Guo, Y.; Tang, J.; Zhang, H.-J.; Chibotaru, L. F.; Powell, A. K. *J. Am. Chem. Soc.* **2011**, *133*, 11948.
(9) Rinehart, J. D.; Long, J. R. *Chem. Sci.* **2011**, *2*, 2078.
(10) Feltham, H. L. C.; Klöwer, F.; Cameron, S. A.; Larsen, D. S.; Lan, Y.; Tropiano, M.; Faulkner, S.; Powell, A. K.; Brooker, S. *Dalton Trans.* **2011**, *40*, 11425.
(11) (a) Waldmann, O. *Inorg. Chem.* **2007**, *46*, 10035. (b) Ruiz, E.; Cirera, J.; Cano, J.; Alvarez, S.; Loose, C.; Kortus, J. *Chem. Commun.* **2008**, 52. (c) Neese, F.; Pantazis, D. A. *Faraday Discuss.* **2011**, *148*, 229.
(12) (a) Ishikawa, N. *Polyhedron* **2007**, *26*, 2147. (b) Gonidec, M.; Luis, F.; Vílchez, À.; Esquena, J.; Amabilino, D. B.; Veciana, J. *Angew. Chem., Int. Ed.* **2010**, *49*, 1623.
(13) See, for example: (a) Brooker, S. *Coord. Chem. Rev.* **2001**, *222*, 33. (b) Brooker, S. *Eur. J. Inorg. Chem.* **2002**, 2535. (c) Hewitt, I. J.; Tang, J.-K.; Madhu, N. T.; Pilawa, B.; Anson, C. E.; Brooker, S.; Powell, A. K. *Dalton Trans.* **2005**, 429. (d) Croucher, P. D.; Klingele, M. H.; Noble, A.; Brooker, S. *Dalton Trans.* **2007**, 4000. (e) de Geest, D. J.; Noble, A.; Moubaraki, B.; Murray, K. S.; Larsen, D. S.; Brooker, S. *Dalton Trans.* **2007**, 467. (f) Kitchen, J. A.; Brooker, S. *Dalton Trans.* **2010**, *39*, 3358. (g) Cameron, S. A.; Brooker, S. *Inorg. Chem.* **2011**, *50*, 3697.
(14) Gallant, A. J.; MacLachlan, M. J. *Angew. Chem., Int. Ed.* **2003**, *42*, 5307.
(15) Akine, S.; Taniguchi, T.; Nabeshima, T. *Tetrahedron Lett.* **2001**, *42*, 8861.
(16) Feltham, H. L. C.; Brooker, S. *Coord. Chem. Rev.* **2009**, *253*, 1458.
(17) Akine, S.; Sunaga, S.; Taniguchi, T.; Miyazaki, H.; Nabeshima, T. *Inorg. Chem.* **2007**, *46*, 2959.
(18) (a) Efthymiou, C. G.; Stamatatos, T. C.; Papatriantafyllopoulou, C.; Tasiopoulos, A. J.; Wernsdorfer, W.; Perlepes, S. P.; Christou, G. *Inorg. Chem.* **2010**, *49*, 9737. (b) Chilton, N. F.; Langley, S. K.; Moubaraki, B.; Murray, K. S. *Chem. Commun.* **2010**, *46*, 7787.
(19) Yamashita, A.; Watanabe, A.; Akine, S.; Nabeshima, T.; Nakano, M.; Yamamura, T.; Kajiwara, T. *Angew. Chem., Int. Ed.* **2011**, *50*, 4016.
(20) Feltham, H. L. C.; Clérac, R.; Powell, A. K.; Brooker, S. *Inorg. Chem.* **2011**, *50*, 4232.
(21) (a) Akine, S.; Taniguchi, T.; Nabeshima, T. *Tetrahedron Lett.* **2001**, *42*, 8861. (b) Akine, S.; Taniguchi, T.; Nabeshima, T. *J. Am. Chem. Soc.* **2006**, *128*, 15765.
(22) Sheldrick, G. M. *Acta Crystallogr., Sect. A: Found. Crystallogr* **2008**, *A64*, 112.
(23) Housecroft, C. E.; Sharpe, A. G. *Inorganic Chemistry*, 2nd ed.; Pearson Education Limited: Essex, England, 2005.
(24) Addison, A. W.; Rao, T. N.; Reedijk, J.; van Rijn, J.; Vershoor, G. C. *J. Chem. Soc., Dalton Trans.* **1984**, 1349.
(25) (a) Borrás-Almenar, J. J.; Clemente-Juan, J. M.; Coronado, E.; Tsukerblat, B. S. *Inorg. Chem.* **1999**, *38*, 6081. (b) Borrás-Almenar, J. J.; Clemente-Juan, J. M.; Coronado, E.; Tsukerblat, B. S. *J. Comput. Chem.* **2001**, *22*, 985.
(26) Aquilante, F.; De Vico, L.; Ferre, N.; Ghigo, G.; Malmqvist, P. A.; Neograd y, P.; Pedersen, T. B.; Pitonak, M.; Reiher, M.; Roos, B. O.; Serrano-Andres, L.; Urban, M.; Veryazov, V.; Lindh, R. *J. Comput. Chem.* **2010**, *31*, 224.
(27) Lines, M. E. *J. Chem. Phys.* **1971**, *55*, 2977.
(28) (a) Ungur, L.; Van den Heuvel, W.; Chibotaru, L. F. *New J. Chem.* **2009**, *33*, 1224. (b) Chibotaru, L. F.; Ungur, L. Leuven, 2006.
(29) (a) Gojon, E.; Gaillard, J.; Latour, J.-M.; Laugier, J. *Inorg. Chem.* **1987**, *26*, 2046. (b) Akine, S.; Matsumoto, T.; Taniguchi, T.; Nabeshima, T. *Inorg. Chem.* **2005**, *44*, 3270. (c) Gojon, E.; Greaves, S. J.; Latour, J.-M.; Povey, D. C.; Smith, G. W. *Inorg. Chem.* **1987**, *26*, 1457. (d) Gojon, E.; Latour, J.-M. *J. Chem. Soc., Dalton Trans.* **1990**, 2043.
(30) Chibotaru, L. F.; Ungur, L.; Aronica, C.; Elmoll, H.; Pilet, G.; Luneau, D. *J. Am. Chem. Soc.* **2008**, *130*, 12445.
(31) Guo, F.-S.; Liu, J.-L.; Leng, J.-D.; Meng, Z.-S.; Lin, Z.-J.; Tong, M.-L.; Gao, S.; Ungur, L.; Chibotaru, L. F. *Chem.—Eur. J.* **2011**, *17*, 2458.
(32) Ungur, L.; Chibotaru, L. F. *Phys. Chem. Chem. Phys.* **2011**, *13*, 20086.
(33) Ruiz, E.; Cano, J.; Alvarez, S.; Alemany, P. *J. Comput. Chem.* **1999**, *20*, 1391.
(34) Neese, F. *ORCA. An Ab Initio, Density Functional and Semiempirical Program Package*, Version 2.9; Universität Bonn: Bonn, Germany, 2010.
(35) Shoji, M.; Koizumi, K.; Kitagawa, Y.; Kawakami, T.; Yamanaka, S.; Okumura, M.; Yamaguchi, K. *Chem. Phys. Lett.* **2006**, *432*, 343.
(36) Kahn, O.; *Molecular Magnetism*; VCH Publishers Inc.: New York, 1993.
(37) Ruiz, E.; Rodríguez-Fortea, A.; Alvarez, S. *Inorg. Chem.* **2003**, *42*, 4881.